University of Nebraska - Lincoln

DigitalCommons@University of Nebraska - Lincoln

David Sellmyer Publications   Research Papers in Physics and Astronomy

7-2009

Spectroscopic investigations on Polypropylene-Carbon Nanofiber Composites: I. Raman and Electron Spin Resonance Spectroscopy

Mircea Chipara
University of Texas Pan American, mchipara@utpa.edu

John R. Villarreal
University of Texas Pan American

Magdalena Dorina Chipara
University of Texas Pan American, dorina.chipara@utrgv.edu

Karen Lozano
University of Texas Pan American

Alin Cristian Chipara
University of Texas Pan American, cristian.chipara@gmail.com

See next page for additional authors

Follow this and additional works at: https://digitalcommons.unl.edu/physicssellmyer

Part of the Physics Commons

Authors

Mircea Chipara, John R. Villarreal, Magdalena Dorina Chipara, Karen Lozano, Alin Cristian Chipara, and
David J. Sellmyer

Spectroscopic investigations on Polypropylene-Carbon Nanofiber Composites:
I. Raman and Electron Spin Resonance Spectroscopy

Mircea Chipara,[1] John R. Villarreal,[2] Magdalena Dorina Chipara,[1]
Karen Lozano,[3] Alin Cristian Chipara,[2, 3] David J. Sellmyer[4]

[1] Department of Physics and Geology, University of Texas Pan American, Edinburg , Texas 78541

[2] Department of Chemistry, University of Texas Pan American, Edinburg, Texas 78541

[3] Department of Mechanical Engineering, University of Texas Pan American, Edinburg, Texas 78541

[4] Department of Physics and Astronomy, University of Nebraska–Lincoln, Lincoln, Nebraska 68588

Corresponding author − Mircea Chipara, Department of Physics and Geology,
University of Texas Pan American, Edinburg, Texas 78541; email mchipara@utpa.edu

Abstract
Isotactic polypropylene-vapor grown carbon nanofiber composites containing various fractions of carbon nanofibers, ranging from 0 to 20 wt %, have been prepared. Raman spectroscopy was used to analyze the effect of the dispersion of carbon nanofibers within polypropylene and the interactions between carbon nanofibers and macromolecular chains. The as-recorded Raman spectra have been successfully fitted by a linear convolution of Lorentzian lines. Changes of the Raman lines parameters (position, intensity, width, and area) of polypropylene and carbon nanofibers were analyzed in detail. The Raman spectra of the polymeric matrix—at low concentrations of nanofibers—show important modifications that indicate strong interactions between carbon nanofibers and the polymeric matrix reflecting by vibrational dephasing of macromolecular chains. The Raman spectrum of carbon nanofibers is sensitive to the loading with carbon nanofibers, showing changes of the resonance frequencies, amplitudes, and width for both D- and G-bands. Raman data reveals the increase of the disorder, as the concentration of carbon nanofibers is increased. The presence of the typical ESR line assigned to conducting electrons delocalized over carbon nanofibers is confirmed and the presence of a spurious magnetic line due to catalyst's residues is reported.

Keywords: carbon nanotubes, ESR/EPR, nanocomposites, poly(propylene), Raman spectroscopy

Introduction

Carbon nanotubes have remarkable properties such as huge Young modulus,[1, 2] large strength,[2] high-thermal conductivity,[3] and good electrical conductivity.[4] Characterized by a very high aspect ratio,[5] carbon nanotubes have been perceived as excellent fillers for improved lightweight materials with enhanced structural capabilities and/or multifunctional materials.[6, 7] Although carbon nanofibers have remarkable physical properties (not as impressing as single and multiwalled carbon nanotubes) they are significantly cheaper providing a cost ef-

ficient solution to polymer-based nanocomposites.[8] The dispersion of carbon nanotubes and nanofibers within polymeric matrices improves the mechanical, thermal, and electrical capabilities of the pristine polymeric matrices adding eventually new properties such as electrical conductivity.[4-8]

This research is divided into two parts: the first focused on Raman and electron spin resonance (ESR) spectroscopy of vapor grown carbon nanofibers (VGCNF) dispersed within isotactic polypropylene (iPP), and the second concentrated on wide angle X-ray scattering (WAXS), and differential scanning calorimetry (DSC). The study aims to a better understanding of the interactions between VGCNFs and iPP adding precision and rigor to the existing literature.[9-16] The second part of the study will inspect the effect of VGCNF on the crystallinity of the polymeric matrix. Preliminary investigations on the morphology and thermal stability of iPP-VGCNF, performed on the same samples, have been reported elsewhere.[15] Rich and unexpected information on the interaction between VGCNF and iPP was extracted from thermogravimetric analysis (TGA) measurements, confirming the formation of an interface between iPP and VGCNF and revealing the complex structure of this interface. A thin hard layer has been tentatively identified and assigned to polymer segments captured by the nanofibers at such small distances that the van der Waals interaction between these molecules and the nanofiber is comparable with the bond energy that links covalently the molecules in the polymer.[15] The presence of a soft layer that extends from the interface nanofiber - polymer at distances comparable with the radius of gyration of polypropylene was also reported.[16] As TGA data suggested a more complicated structure of the interface between VGCNFs and macromolecular chains (iPP), additional investigations were initiated to obtain further experimental evidence for these findings.

The first part of this article concentrates of Raman spectroscopy investigations of iPP-VGCNF composites. This analysis is traditionally focused on the Raman lines due to the filler (VGCNFs).[9-16] The original aspect of this study derives from the fact that the analysis of Raman spectra includes both the polymeric matrix and the filler. This required the computer deconvolution of the full Raman spectrum and resulted in a more accurate estimation of Raman lines positions, amplitudes, widths, and areas. The second part of this article analyzes ESR spectroscopy results. This experimental technique is not yet frequently used to investigate carbon nanotubes and carbon nanofiber composites.

Polypropylene is a macromolecule with a simple repeating unit and various tacticities defined by the position of the methyl group relative to the polymer backbone.[17] iPP is obtained by the addition of monomers with all substituents placed on the same side of the backbone chain. iPP is a semicrystalline polymer with a tendency to take helix like configuration (repeating unit built of three monomers related each to other by a three-fold helix axis).[17] The Raman spectrum of iPP is complex, consisting of 25 parallel and polarized modes (A modes) and 52 perpendicular and depolarized (E) modes.[18, 19] The analysis of Raman spectra of polypropylene is complicated by the fact that in most cases A and E modes are mixed.[18, 19] Certain Raman modes are not significantly affected by the configuration and conformation of macromolecular chains. For example, the Raman lines located at 1152, 1034, 900, and 841 cm^{-1} in molten isotactic and sindiotactic polypropylene are coincident or almost coincident.[17-19] As expected, some other Raman lines are characteristic either to the sindiotactic or isotactic addition of monomers.[17]

Pristine polymers such as iPP show no ESR spectra.[20] Under certain circumstances, residual ESR spectra may point either to catalyst residues or to trapped free radicals generated by mechanical, thermal, or oxidative processes.[20] VGCNFs show ESR spectra almost identical to the ESR spectra of carbon nanotubes.[21] Typically, the ESR spectrum of carbon nanotubes contains several contributions[22-24]; a very broad line characterized by $g > 2.00$ assigned to catalyst's impurities (magnetic nanoparticles), a narrow line (sometimes asymmetric) located near $g = 2.0023$ and assigned to conducting electrons delocalized over carbon nanotubes or carbon nanofibers. The ESR line originating from conducting electrons delocalized over carbon nanotubes or carbon nanofibers is temperature independent. ESR spectra may be used to assess the average orientation or carbon nanotubes/nanofibers within polymeric matrices.[21] Eventually, another narrow line assigned to graphitic carbon has been reported[22-24] around $g = 2.0023$.

Experimental Methods

iPP-VGCNF nanocomposites were obtained by high-shear mixing of iPP (Marlex HLN-120-01; Philips Sumika Polypropylene Company, density 906 kg/m^3; more de-
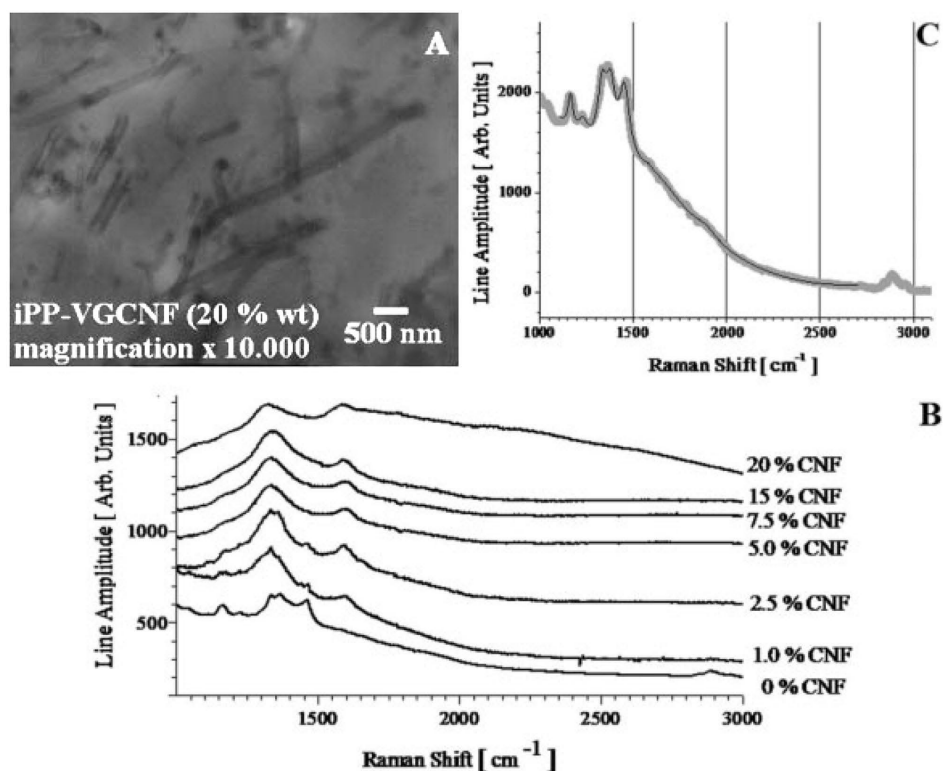
Figure 1. A: TEM photo of iPP-VGCNF composite; **B**: Raman spectra of iPP filled with various amounts of VGCNFs (expressed in wt %); and **C**: The best fit of Raman spectrum in the range 1000-2800 cm^{-1} for the pristine polymer.

tails about the polymeric matrix are available at http://www.cpchem.com/enu/polypropylene_tl_technical_library.asp) with various amounts of VGCNFs (PR-24AG; Pyrograf Products, Inc.) by utilizing a HAAKE Rheomix at 65 rpm and 180 °C for 9 min followed by an additional mixing of 5 min at the same temperature and at 90 rpm. The as-received VGCNFs have been chemically treated as reported elsewhere[15] to debundle and purify the nanofibers. Composites loaded with various amounts of VGC-NFs ranging between 0 and 20 wt % have been prepared. Scanning electron microscopy confirmed the homogeneous distribution of CNFs within the polymeric matrix see Figure 1(A).[15] Raman spectroscopy analysis has been performed by using a Bruker Sentera dispersive Raman microscope spectrometer equipped with a 785 nm laser diode. ESR measurements have been carried out at room temperature with a Bruker Elexsys spectrometer, operating in the X-band (~9 GHz).

Results And Discussions

The weak intensity of the Raman lines due to polypropylene in polymer-nanotube composites has been recognized by several authors.[10-13] This section focuses on the analysis of the Raman spectra of both VGCNF and iPP in composites containing various amounts of VGCNFs, aiming to extract new information regarding the interaction of macromolecular chains with the nanofiller from an exhaustive analysis of Raman spectra.

The Raman spectra of iPP-VGCNF, for different loadings with VGCNFs (ranging from 5 to 20 wt %, VGCNF), are shown in Figure 1(B). The as-recorded spectra are rather complex; the contribution of iPP dominates Raman spectra of iPP-VGCNFs that contains a low concentration of VGCNFs. It is important to notice that the contributions of iPP are expected to dominate the Raman spectra characterized by shifts smaller than 1200 cm^{-1}.[19, 25] The Raman spectra in the range 1100-2800 cm^{-1} have been simulated by a convolution of up to 11 symmetric Lorentzian lines. Figure 1(C) demonstrates the good agreement between the fitted spectrum (black and narrow line) and the as-recorded spectrum (gray and broad line).

For an exhaustive analysis of Raman lines assigned to the polymeric matrix, several domains were investigated in detail (see Figures 2 and 3). As observed from Figure 2(A), the absence of a very strong Raman line lo-
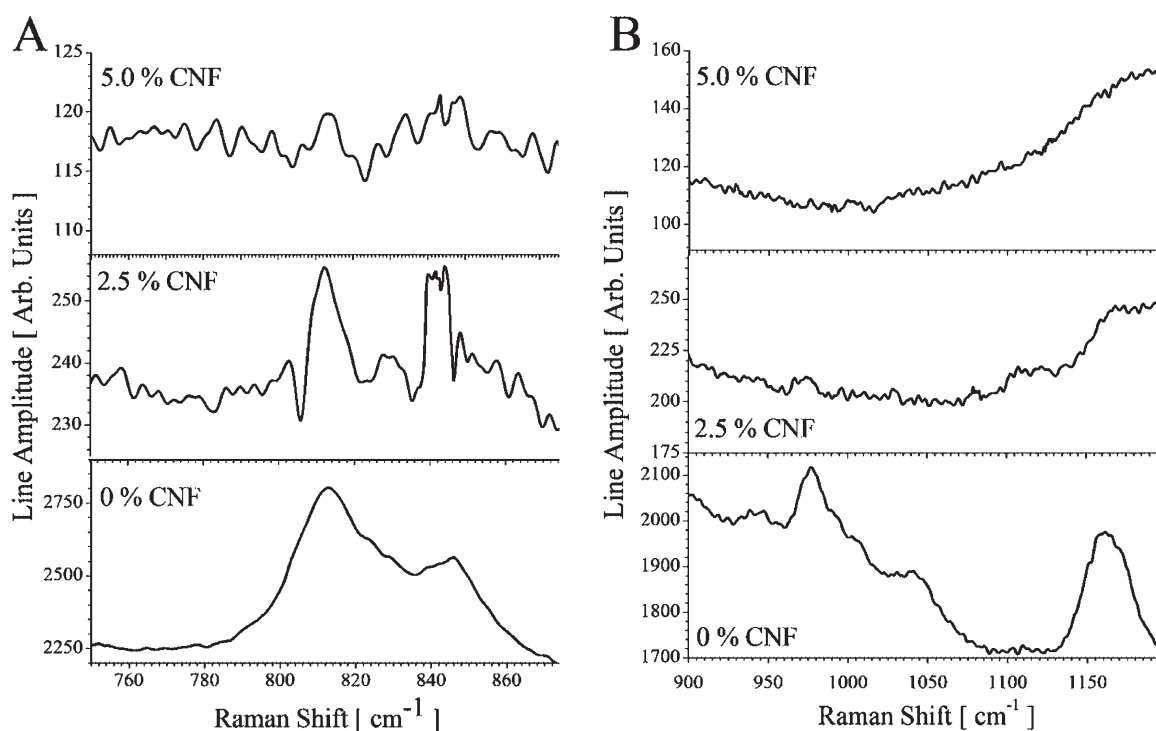
Figure 2. The Raman spectra of iPP-VGCNF composites for Raman shifts ranging between 750 and 900 cm^{-1} (left panel) and 900 and 1200 cm^{-1} (right panel), respectively.

cated at 850 cm^{-1} rules-out the possibility of sindiotactic-like structures.[18, 19] The degree of crystallinity of iPP may be inferred from Raman spectra within a three-phase model[19] that implies a crystalline phase responsible for the Raman line located at 808 cm^{-1}, a defected phase containing mostly helical chains identified by the Raman line located at 840 cm^{-1}, and a melt-like structure assigned to amorphous polypropylene and assigned to the line noticed at 830 cm^{-1}.[19] As noticed from Figure 3 (bottom spectrum), the as-recorded Raman lines were observed at slightly higher Raman shifts. This may reflect the dispersive nature of these lines (the laser radiation used in this experiment had a frequency of 785 nm, while the aforementioned line positions were reported for a laser frequency of 633 nm).[19] Higher concentration of VGCNFs distorts completely the polymeric matrix, up to the point at which above 5 wt %. VGCNFs the lines of the polymeric matrix, expected to be observed in the range of 725-875 cm^{-1} become invisible. The Raman line located at 844 cm^{-1} has been assigned to short range order vibrations involving about 13 units, whereas the line located at 811 cm^{-1} has been assigned to short range vibrations involving 15 units.[26] These lines are rapidly disappearing as the concentration of VGCNFs is increased,

indicating strong distortions in the polymer structure triggered by the interaction between the polymeric matrix and VGCNFs.

As is noticed from Figure 3, the Raman line located at 2841 cm^{-1} assigned to CH$_2$ symmetric stretching ($d+$) is visible for pristine iPP but disappears completely on
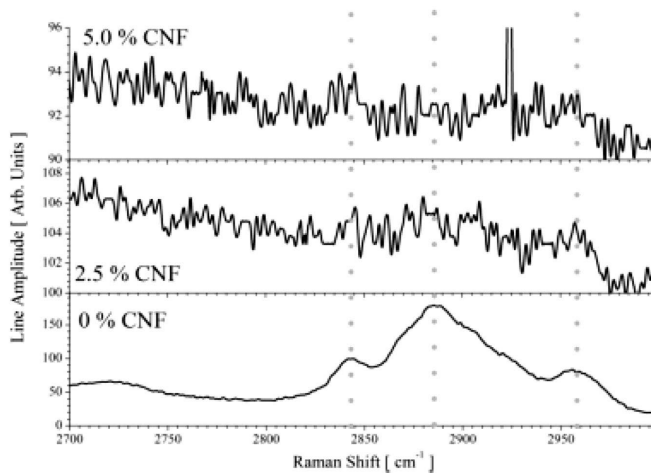

Figure 3. The Raman spectra of some iPP-VGCNF composites for Raman shifts ranging between 2700 and 3000 cm^{-1}.
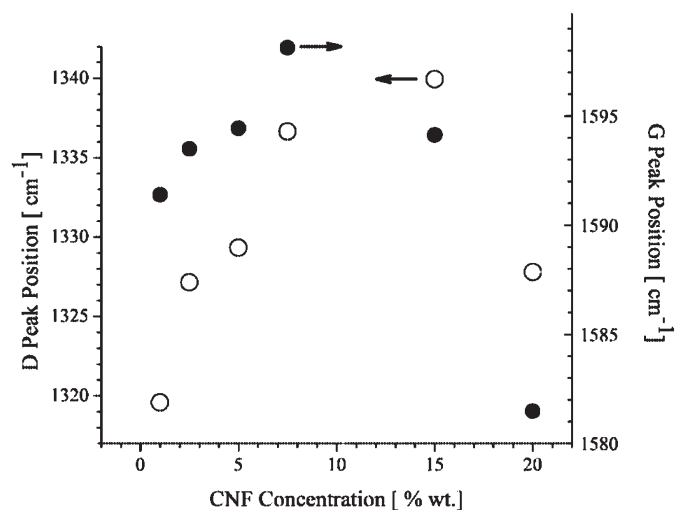
Figure 4. The dependence of the D- and G-lines position on the concentration of VGCNF.

Figure 5. The effect of the concentration of VGCNF on the width of the D- and G-bands (top panel), on the ratio between the amplitude of the D- and G-bands (bottom panel, left axis) and on the estimated cluster correlation length (bottom panel, right axis).

loading with VGCNF. The Raman line assigned to CH_2 asymmetric stretching (*d*-) expected at 2920 cm^{-1} is significantly weaker than the symmetric one. The symmetric CH_3 stretching for iPP splits into two lines, a weaker Raman line located at 2870 cm^{-1} (not observed in the spectrum of pristine iPP) and a stronger line located at 2883 cm^{-1} (see Figure 3). The asymmetric stretch (*r*-) splits into an out of the plane stretch at 2953 cm^{-1} and an in-plane stretch at 2962 cm^{-1}. In Figure 3, these line are merged into a single broad Raman line suggesting a random distribution of crystallites. From Figure 3, it is noticed that the CH_2 vibrations are more affected by the loading with carbon nanofibers than the CH_3 vibrations.[19, 26, 27] This indicates a strong interaction of VGCNFs with the polymeric backbone rather than with the CH_3 side group.

The addition of VGCNF results in a sudden decrease of the intensity of all Raman lines assigned to iPP. This drop does not necessarily imply that the degree of crystallinity of the polymeric phase in iPP-VGCNF composites decreases on loading with VGCNF as the degree of crystallinity is controlled by the area of the peak rather than by its intensity. It is noticed that the width of iPP Raman lines increases very fast as VGCNFs are introduced within the polymeric matrix. Hence, even if the intensities of the Raman lines assigned to iPP are decreased below detection, the simultaneous broadening of these lines may compensate for the drop in the line intensities of Raman spectra. Under these circumstances, the load-
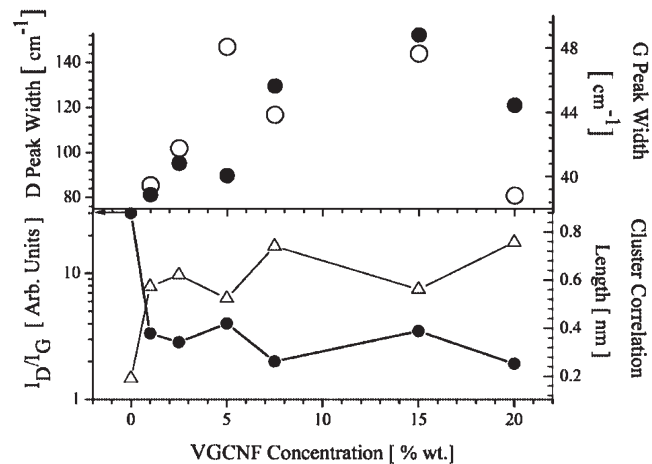
ing of iPP with VGCNFs (up to about 2.5 % VGCNFs) changes dramatically the dynamical aspects of Raman spectra confined in their line width, but do not result necessarily in a decrease of the crystallinity degree as the concentration of VGCNFs in iPP is increased. However, the observed appearance and increase of helical macromolecular chains suggests a decrease of the crystallinity degree of the iPP phase. This agrees with TGA data that demonstrated the formation of the iPP-VGCNF interface[15]; we are speculating that most of these chains are wrapped around VGCNFs contributing to the soft iPP-VGCNF interface.

Several lines, originating from the VGCNF dispersed within the polymeric matrix were easily identified; first-order Raman spectra include [9-16, 14, 28-32] the line located at about 1320 cm^{-1}, identified as the D-mode and the line located at 1590 cm^{-1}, identified as the G-mode. The D-mode is dispersive, that is, the Raman line position depends on the frequency of the laser beam. As observed from Figure 1, the D-line dominates all Raman spectra of iPP-VGCNF composites suggesting that VGCNFs are disordered. As shown in Figure 4, the position of the D-line shifts toward higher wavelength as the concentration of VGCNF is increased from 0 wt % to about 10 wt %. Above this concentration, the position of the D-line starts to decrease as the concentration of VGCNFs is increased. An analogous dependence has been noticed for the dependence of the width of the D-line on the loading with

VGCNFs (see the top panel of Figure 5, left axis). The same dependence of the D-line position and amplitude has been reported in iPP loaded with single wall carbon nanotubes (SWCNTs) and assigned to the intercalation of macromolecular chains among VGCNFs. Similar data have been reported in the case of PP loaded with SW-CNTs.[10, 11, 30] The increase of the D-line position as the concentration of VGCNFs/SWCNTs is increased up to 10 % was assigned to the intercalation of macromolecular chains among filler's particles, suggesting an increase of the debundling efficiency of VGCNFs during the processing step. The decrease of the D-line position as the concentration of VGCNFs/SWCNTs is further increased (above 15 wt % VGCNFs) was assigned to the weak aggregation of VGCNFs.[11, 12]

The G-line is wide and intense, suggesting in-plane structural disorder.[9-16, 14, 28-32]. Within the experimental errors neither G-band splitting nor the change in the shape of this band were noticed.[15-17] This suggests that the electrical conductivity of VGCNF was not very high. The dependence of the G-line position and width is qualitatively similar to the dependence of the D-line on the Raman line position and width (see Figures 4 and 5). The ratio between the amplitude of the D- and G-lines is frequently used to characterize the degree of disorder within CNTs. As may be noticed from the right panel of Figure 5, the ratio of the amplitude of the D- and G-lines amplitude is increasing as the concentration of VGCNFs is increased, indicating a more pronounced disorder within carbon nanofibers as their concentration within the polymeric matrix is increased. The averaged in-plane crystallite size, L, or the so-called cluster correlation length is proportional to the ratio of the amplitudes of G- and D-lines. As observed from Figure 5, L decreases as the concentration of carbon nanofibers is increased, confirming the decrease of the crystallite size (and the increase of the disorder).

Second-order Raman lines[14, 28-32] are also noticed (see Figure 1); the line located at about 2600 cm^{-1} has been assigned to the D* mode, whereas the 2Γ mode located about 3200 cm^{-1} has not been observed. The D″ line reported in some carbon nanofibers and located at about 1500 cm^{-1} has not been observed.[14, 28, 29, 33] A weak line located between 1420 and 1470 cm^{-1}, has been noticed and tentatively assigned to band modes about K or M points.[29] These lines are enhanced as the loading with VGCNF is increased. However, the overlap of this line with a line due to the polymeric matrix makes difficult for a detailed analysis of these resonances.
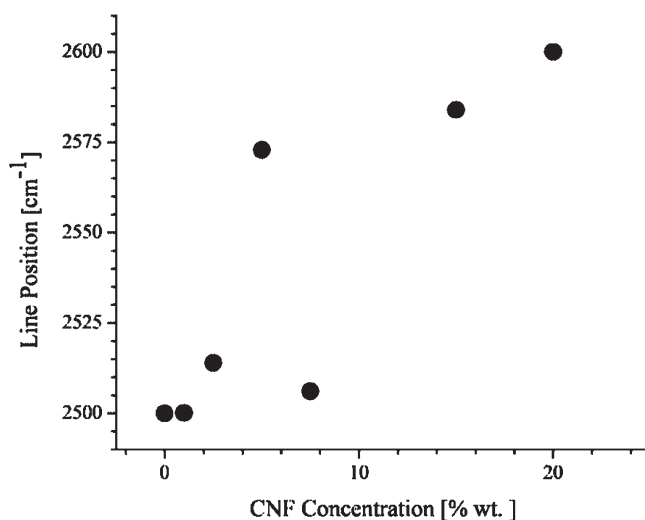

Figure 6. The effect of VGCNF concentration of the Raman line located between 2500 and 2600 cm^{-1}.

VGCNFs exhibit broader Raman lines than SWCNTs and accordingly we were not able to deconvolute the Raman lines observed at 1549 and 1589 cm^{-1}.[12, 13] Because of the wide distribution of VGCNFs diameters, no Raman line has been observed in the radial breathing range (100–500 cm^{-1}).

Pristine polypropylene exhibits a peak located at about 2500 cm^{-1}. By increasing the loading with carbon nanofibers this peak disappears and for carbon nanofiber concentrations in excess of 5 % VGCNF, a peak located at about 2550 cm^{-1} has been noticed and assigned to the D* mode. As may be inferred from Figure 6, the position of this peak depends on the loading with VGCNFs. Taking into account that the position of this peak may be related to the internal stresses exerted on VGCNFs, it is speculated that the VGCNFs experiences large local stresses due to the thermomechanical processing, and that these internal stresses are partially frozen within iPP-VGCNFs composites.. Accordingly, the concentration of VGCNFs is increased the local pressure increases shifting the D* lines to higher wavenumbers (see Figure 6).[31]

The ESR spectra of iPP-CNF composites are shown in Figure 7. The resonance spectrum located near the g = 2.00 (see the top panel of Figure 7) has been assigned to conducting electrons delocalized over VGCNFs. However, for pristine iPP, subjected to the same thermomechanical treatment a very weak ESR spectrum has been observed and assigned to free radicals generated by thermomechanical scissions of macromolecular chains during the preparation and processing of samples.[20]
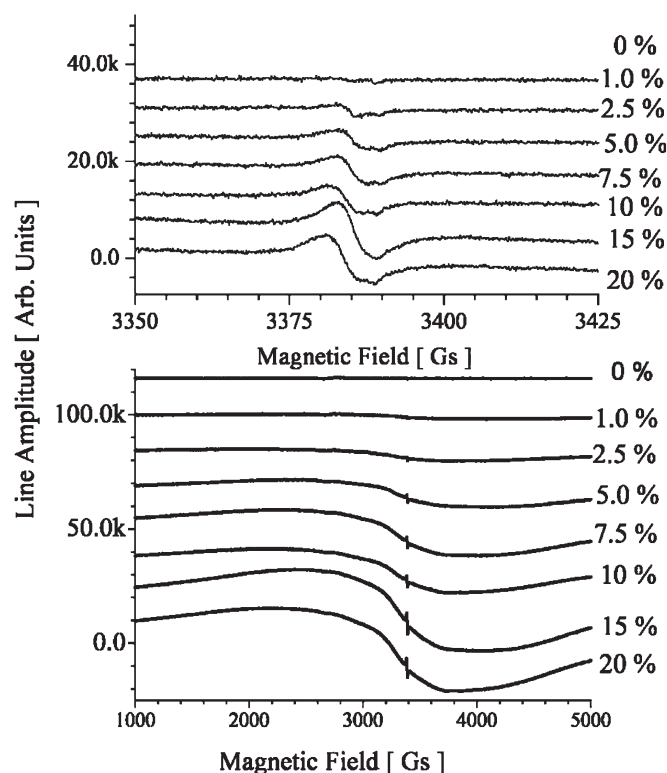
Figure 7. ESR spectra of iPP-VGCNF composites. Upper panel shows in detail the ESR spectrum of the composite around the $g = 2.00$ value, whereas the bottom panel shows also the broad line due to catalyst's impurities.

The full ESR spectrum of iPP-CNF, in the X-band (~9 GHz), at room temperature is shown in the bottom panel of Figure 7. The broad and intense line originates from magnetic nanoparticles (catalyst's residues). The analysis was focused on the narrow line located close to $g = 2.00$ and assigned to conducting electrons.[21-24] This line has been successfully fitted with a single Lorentzian. For metallic nanofibers, an asymmetrical Dysonian-line resonance line shape was expected[22] (due to the skin effect). The actual (symmetrical) shape of the narrow ESR line suggests that the nanofibers used to obtain these nanocomposites have a relatively low-electrical conductivity, in agreement with Raman's findings. The free-radical concentration in ESR spectroscopy is proportional to the double integral of the resonance spectrum.[20] For a simple Lorentzian line, the double integral of the resonance spectrum, is proportional to the amplitude of the ESR line and the square of the peak to peak linewidth.[20,21] As it is observed from Figure 8, the intensity of the resonance line located near $g = 2.00$ and the double integral of this line are increasing as the concentration of VGCNF is increased, confirming that this signal originates from VGCNF.
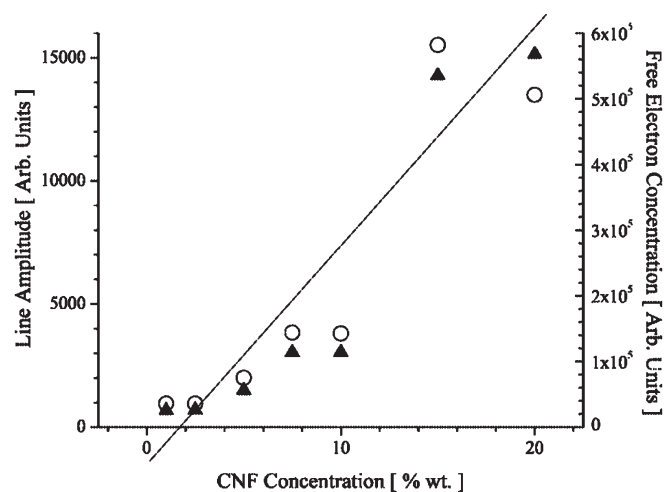

Figure 8. The dependence of the amplitude of the ESR line assigned to conducting electrons delocalized over VGCNFs on the concentration of VGCNFs (left axis) and the dependence of the concentration of free electrons on the concentration of VGCNF.

Conclusions

Both polymers and carbon nanotubes/nanofibers exhibit Raman spectra. In the case of iPP-VGCNF composites, the loading of the polymeric matrix by VGCNFs is associated with a rapid drop of the intensity of the Raman lines assigned to iPP accompanied by a fast broadening of these lines. This fast vibrational dephasing of macromolecular chain demonstrates the strong interaction between VGCNFs and iPP chains, making difficult the Raman spectroscopy study of both polymeric matrix and filler over a wide range of VGCNFs' concentrations. The loading of iPP with VGCNFs resulted in complex modifications of the Raman spectra of the polymeric matrix, which indicates the wrapping of macromolecular chains around VGCNFs and agrees with previously reported TGA data, suggesting a decrease in the overall degree of crystallinity of the polymeric matrix.[15] Consequently, Raman spectroscopy was not capable to provide an accurate estimation of the degree of crystallinity of iPP-CNF composites. No evidence concerning the potential oxidation of polypropylene during the thermomechanical processing of the composites was observed from Raman studies.[33] The second part of this article, will concentrate on the crystallinity of iPP-VGCNFs, as revealed by DSC and WAXS investigations.

The Raman spectra of VGCNFs show the usual dependence on the concentration of VGCNFs. An increase

in the degree of disorder of VGCNFs as their concentration is increased was noticed from the dependence of the ratio between the amplitude of the D- and G-modes on the concentration of VGCNF. The effect of the loading with carbon nanofiber on the D* Raman line suggests that the nanofibers are subjected to important local stresses and these stresses increase as the concentration of carbon nanofibers is increased.[32] The reported changes on the D- and G-band position and width, derived from the introductions of VGCNFs are identical to the modifications reported in iPP filled with SWCNTs and multi-walled carbon nanotubes.[9-14]

ESR spectroscopy revealed the generation of free radicals within the pristine polymer during its processing, confirmed the presence of catalysts residues, and quantified the free electrons delocalized over the conducting domains of carbon nanofibers. Although the processing technique used to obtain iPP-VGCNFs nanocomposites resulted in free-radical generation, Raman spectroscopy ruled-out conformational and tacticity modifications of the polymeric matrix. The potential reduction of the degree of crystallinity of iPP on loading with VGCNF may express the consequence of the processing step, when the combined effect of temperature and mechanical stresses and the potential presence of oxygen traces may result in the degradation of the macromolecular chain (predominant scission reactions). The increase of the concentration of chain ends may contribute to a weak decrease of the overall crystallinity degree of iPP phase.

References

1. Yu, M. F.; Lourie, O.; Dyer, M. J.; Moloni, K.; Kelly, T. F.; Ruoff, R. S. *Science* 2008, **287**, 637-640.

2. Terrones, M.; Grobert, N.; Olivares, J.; Zhang, J. P.; Terrones, H.; Kordatos, K.; Hsu, W. K.; Hare, J. P.; Townsend, P. D.; Prassides, K.; Cheetham, A. K.; Kroto, H. W.; Walton, D. R. M. *Nature* 1997, **388**, 52-55.

3. Che, J.; Çagin, T.; Goddard, W. A. *Nanotechnology* 2000, **11**, 65-69.

4. Ebbesen, T. W.; Lezec, H. J.; Hiura, H.; Bennett, J. W.; Ghaemi, H. F.; Thio, T. *Nature* 1996, **382**, 54-56.

5. Wong, S. S.; Joselevich, E.; Woolley, A. T.; Cheung, C. L.; Lieber, C. M. *Nature* 1998, **394**, 52-55.

6. Moniruzzaman, M.; Winey, K. I. *Macromolecules* 2006, **39**, 5194-5205.

7. Thostenson, E. K.; Ren, Z.; Chou, T. W. *Compos Sci Technol* 2001, **61**, 1899-1912.

8. Ajayan, P. M.; Schadler, L. S.; Giannaris, C.; Rubio, A. *Adv Mater* **12**, 750-753.

9. Bhattacharyya, A. R.; Sreekumar, T. V.; Liu, T.; Kumar, S.; Ericson, L. M.; Hauge, R. H.; Smalley, R. E. *Polymer* 2003, **44**, 2373-2377.

10. Seo, M. K.; Lee, J. R.; Park, S. J. *Mater Sci Eng A* 2005, **404**, 79-84.

11. Vassiliou, A.; Bikiaris, D.; Chrissafis, K.; Paraskevopoulos, K. M.; Stavrev, S. Y.; Docoslis, A. *Compos Sci Technol* 2008, **68**, 933-943.

12. Valentini, L.; Biagiotti, J.; López-Manchado, M. A.; Santucci, S.; Kenny, J. *Polym Eng Sci* 2004, **44**, 303-311.

13. Lee, G. W.; Jagannathan, S.; Chae, H. G.; Minus, M. L.; Kumar, S. *Polymer* 2008, **49**, 1831-1840.

14. Valentini, L.; Biagiotti, J.; López-Manchado, M. A.; Santucci, S.; Kenny, J. *Compos Sci Technol* 2003, **63**, 1149-1153.

15. Chipara, M. D.; Lozano, K.; Hernandez, A.; Chipara, M. T. G. A. *Polym Degrad Stab* 2008, **93**, 871-876.

16. Zhao, Q.; Wagner, H. D. *Phil Trans R Soc Lond A* 2004, **362**, 2407-2424.

17. Masetti, G.; Cabassi, F.; Zerbi, G. *Polymer* 1980, **21**, 143-152.

18. Gatos, K. G.; Kandilioti, G.; Galiotis, C.; Gregoriou, V. G. *Polymer* 2001, **45**, 4453-4464.

19. Nielsen, A. S.; Batchelder, D. N.; Pyrz, N. *Polymer* 2002, **43**, 2671-2676.

20. Ranby, B.; Rabek, J. F. *ESR Spectroscopy in Polymer Research*; Springer-Verlag: Berlin, 1977.

21. Chipara, M.; Lozano, K.; Chipara, M. D. *Carbon* 2007, **45**, 2692-2716.

22. Chipara, M.; Iacomi, F.; Zaleski, J. M.; Bai, J. B. *J Optoelectron Adv Mater* 2006, **8**, 820-824.

23. Chipara, M.; Zaleski, J. M.; Hui, D.; Pan, N. *J Polym Sci Part B: Polym Phys* 2005, **43**, 3406-3412.

24. Chipara, M.; Lozano, K.; Wilkins, R.; Barrera, E. V.; Pulikkathara, M. X.; Penia-Para, L.; Chipara, M. D. *J Mater Sci* 2008, **43**, 1228-1233.

25. Hahn, T.; Suen, W.; Kang, S.; Hsu, S. L.; Stidham, H. D.; Siedle, A. R. *Polymer* 2001, **42**, 5813-5822.

26. Fraser, G. V.; Hendra, P. J.; Watson, D. S.; Gall, M. J.; Willis, H. A.; Cudby, M. E. A. *Spectrochim Acta 2002* , **29**, 1525-1533.

27. Pae, K. D.; Morrow, D. R.; Sauer, J. A. *Nature* 1966, **211**, 514-515.

28. Bailey, R. T.; Hyde, A. J.; Kim, J. J. *Spectrochim Acta* 1974, **30**, 91-98.

29. Masetti, G.; Cabassi, F.; Zerbi, G. *Thin Solid Films* 2007, **515**, 2958-2964.

30. Thomsen, C. *Phys Rev B* 2000, **61**, 4542-4544.

31. Dresselhaus, M. S. G.; Dresselhaus, G.; Jorio, A.; Souza Filho, A. G.; Pimenta, M. A.; Saito, R. *Acc Chem Res* 2002, **35**, 1070-1078.

32. Martin Ganß, M.; Satapathy, B. K.; Thunga, M.; Weidisch, R.; Pötschke, P.; Jehnichen, D. *Acta Mater* 2008, **56**, 2247-2261.

33. Idriss, B.; Graeme, A. G. *Polym Degrad Stab* 2000, **70**, 269-275.